Fully Lagrangian Approach of Three-Phase Systems for Debris Bed Formation (Part I: DAVINCI experiment)

YoungWoo Son, InSoo Seo, Cheol-O Ahn*
Metariver Technology Co., Ltd., C-716, Moonjeong-SK-V1, 128,
Beobwon-ro, Songpa-gu, Seoul, 05854, Republic of Korea
Corresponding author: coahn@metariver.kr

***Keywords :** DAVINCI experiment, three-phase flow, Discrete Bubble Model (DBM), Moving Particle Semi-implicit (MPS), Discrete Element Method (DEM)

1. Introduction

In case of a severe accident in a light water reactor, the breakup of the melt in water forms a porous debris layer on the bottom of the reactor cavity, and the characteristics of the debris layer are important for the adequate assessment of the coolability of the corium. [1][2][3][4]

To investigate the internal structure of the debris layer and the effect of the bubble generated by decay heat, Kim et al. [1][2] conducted an experimental study using the DAVINCI (Debris Bed Research Apparatus for Validation of the Bubble-Induced Natural Convection Effect Issue) test facility. They studied the structure of the debris layer obtained by injecting air bubbles from the bottom and dropping particles of various sizes into the water tank. In this experiment, the particle column formed by falling particles and the bubble column formed by air injection from the bottom each cause opposite flow and collide, resulting in very complex behavior and ultimately scattering the particles to the bottom. A complex flow field is formed by many bubbles generated by air injection, and it changes the settling path of the settling particles, affecting the formation of the debris bed. Therefore, to accurately predict the shape of the debris bed, it is important to consider the effect of the flow induced by bubbles as well as the behavior of particles of various shapes and sizes.

It is still challenging to simulate the behavior of liquid-solid(particle)-gas(bubble) mixed phases. To implement the behavior of bubbles in water, we adopted the discrete bubble model (DBM) [5]. This method tracks a single bubble as a fixed-size particle and can be applied to the dispersed regime of relatively small bubbles. The various forces applied to a bubble are determined by empirical correlations that take into account its size and shape.

In this study, we propose a method that couples MPS (Moving Particle Semi-implicit method) [7], DEM (Discrete Element Method), and DBM using a fully Lagrangian approach based on the unresolved method to analyze such complex multiphase flows, and the collision between the bubble column and the particle column formed by the falling debris particles were simulated. Since there are quantitative measurement results according to various experimental conditions in the experiments of Kim et al. [1][2], we attempted to compare the simulation results obtained through three-phase simulations using the Lagrangian method with the experimental results.

2. DAVINCI experiment

DAVINCI consists of three major parts: a particle injection system, a test pool, and a PCP module that equips an air injection system. The particle injection system is composed of a funnel and funnel rack to isolate the particle feed from the vibration of the convection flow in the pool. The particles were released by gravity after removing a rubber plug from the nozzle.

Fig. 1. The DAVINCI facility [1][2] (POSTECH)

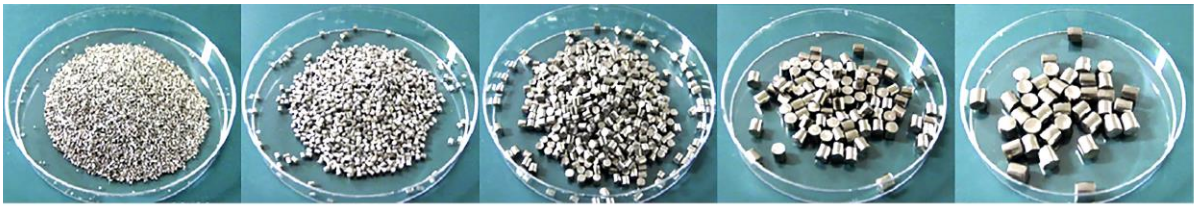

(a) Dv0.92 (b) Dv1.95 (c) Dv3.43 (d) Dv5.72 (e) Dv8.01

Fig. 2. The 5 types of simulant particles

Table 1. The experiment conditions and the information of the particles.

Exp. type		diameter [mm]	height [mm]	sphericity	mass [kg]	release rate [kg/sec.]	No. particles [EA]
SG	Single particle size						
	D_V0.92	0.8	0.8	0.874	2	0.43	574,855
	D_V1.95	1.7	1.7	0.874	2	0.38	64,393
	D_V3.43	3	3	0.874	2	0.3	11,833
	D_V5.72	5	5	0.874	2	0.2	2,552
	D_V8.01	7	7	0.874	2	0.12	930
MT2	A mixture of 5 different particle sizes						
	D_V0.92:D_V1.95:D_V3.43:D_V5.72:D_V8.01 =15:20:30:20:15 (mass fraction)				2.5	0.403	136,319

The test pool was fabricated from a transparent acrylic cylinder to allow visualization. Vapor generation from the hot debris bed was simulated with 32 air chambers in a predetermined air flow rate distribution. [1][2]

Particle sampling catchers were prepared to investigate the local characteristics of the internal structure of debris beds. A stainless steel mesh with an aperture of 0.1 mm was attached to the bottom of the particle sampling catchers to collect all of the settled particles while allowing air bubble penetration. [2]

The particles were made of stainless steel 304, and the density was measured to be about 8,000 kg/m^3. The test SG used single-size particles and the test MT2 used five different particle sizes. The mass fraction of particles in the test condition was designed to simulate corium debris particles from the breakup and fragmentation of the melt jet, using the particle size distribution model of Moriyama et al. [2]

The air flow rate to generate bubbles is denoted as Q_B and five levels were used: 0 lpm, 30 lpm, 50 lpm, 70 lpm, and 90 lpm.

Fig. 1 shows DAVINCI facility, and Fig. 2 shows the test particles used in the experiment. Information about the particles used in the experiment is shown in Table 1. D_V means the equivalent diameter, which is the diameter of a perfect sphere with the same volume as the particle.

3. Numerical method

3.1 Liquid phase

We implemented the MPS method proposed by Koshizuka et al. for the analysis of the continuous phase. MPS [7] basically adopts a semi-implicit algorithm and calculates the pressure field by solving Poisson Pressure Equation (PPE), so the incompressibility of the fluid is ensured and the simulation is stable. In order to consider turbulence, we implemented the Subgrid-scale turbulence model for Large-eddy simulation of MPS introduced by Gotoh et al. and the wall model proposed by Arai et al. and used the Contoured Continuum Surface Force model proposed by Duan et al. to obtain the surface tension force. The Polygon Wall method proposed by Harada et al. and Zhang et al. was used to generate only the surface mesh of a complex wall surface from CAD data and use it directly as a boundary condition.

3.2 Solid phase

For solid particle-based systems, the Discrete Element Method (DEM) has demonstrated excellent capabilities in numerically modeling solid-solid interactions, and coupling DEM with particle-based Lagrangian CFD methods that can handle multiphase flows without the need for interfacial capturing can be a good way to model three-phase flows. [3]

The discrete element method is a numerical analysis for analyzing the behavior of many solid particles and their effects. This method is a Lagrangian method, solves the six-degree-of-freedom equation of motion, and determines the motion of each particle considering all the forces exerted on each particle. The time integration of the equation of motion uses an explicit method using a small-time interval. In the discrete element method, a nonlinear viscoelastic model based on the Hertz-Mindlin contact force model was used to calculate particle-particle and particle-wall collision. The following equation represents the external force acting on a particle.

$$\vec{F}_{s,ext} = \vec{F}_G + \vec{F}_D + \vec{F}_L + \vec{F}_P + \vec{F}_V + \vec{F}_T \quad (1)$$

Each of these forces is assumed to be independent and uncoupled from each other. Detailed expressions of these forces can be found in Table 2.

The drag force of a single spherical particle with a smooth surface can be expressed as a function of the Reynolds number, and various correlations have been proposed by many researchers such as White, Wen and Yu, Di Felice, Cheng, etc. However, when a particle surrounded by many particles behaves inside the flow field, it is necessary to consider the influence of the surrounding particles in obtaining the drag force. In order to consider the swarm effect on the drag coefficient, a dimensionless form of correlation with the volume fraction of the fluid is used. [8] In this study, Di Felice's correlation, which is effective in dense and dilute flow of particles and widely used for drag calculation of spherical and non-spherical particles, was used. By using Di Felice's correlation, the swam effect can be represented by multiplying by the particle's drag coefficient. [8]

In this study, the drag force for non-spherical particles was considered. The drag correlations for a non-spherical particle have been proposed by researchers such as Chien, Haider et al., Ganser, and Hölzer et al., etc. Haider and Levenspiel's correlation, which does not consider crosswise sphericity, was used to calculate the drag force of non-spherical particles.

The hydrodynamic force acting on a particle may be decomposed into components parallel and perpendicular to the direction of the relative motion between the particle and the fluid surrounding it. The former is commonly referred to as the drag force, the latter as the lift force. Regarding the lifting force of spherical particles, Loth, Shi, and Rzehak presented a correlation based on various experimental results and DNS data. Considering the condition of entering the water tank by free fall, in this study, lift force by free rotation was implemented. It should be noted that the non-spherical particles considered in the drag calculations are not taken into account in the lift calculations.

In this study, the particle/bubble induced turbulence model proposed by Sato et al. was implemented. The total viscosity of a liquid is calculated as the sum of molecular viscosity, eddy viscosity due to turbulence, and viscosity induced by particles and bubbles.

3.3 Gas phase

Even considering the recent computing power, numerical simulation of bubble flow is still challenging due to the unstable multiphase interface with high density ratio and high viscosity ratio. Bubble flow, where mass and heat transfer between different phases and severe distortions at the interface exist, is much more complex than single-phase flow or liquid-solid two-phase flow. When solving multiphase flow using numerical analysis, several aspects such as interfacial tracking, discontinuous density fields with high density ratios, and surface tension must be considered. Moreover, these unstable interfaces can break and recombine during flow evolution.

Grid-based analysis methods, such as finite difference method (FDM), finite volume method (FVM), and finite element method (FEM), cannot be applied to the direct simulation of two-phase flows due to discontinuities in the interfacial properties. In order to accurately capture the interface using these methods, several methods such as Volume Of Fluid (VOF), Front-Tracking (FT) method, and Level Set (LS) are used simultaneously. In general, all of these methods focus on handling interfaces between different phases.

In dealing with a large number of bubbles, such as bubble columns, two methods have been proposed, depending on how the disperse phase is handled. The first is to use the Eulerian method based on the grid for both the continuous phase and the disperse phase (E-E), and the other is to use the Eulerian method based on the grid for the continuous phase and the Lagrangian method for the disperse phase (E-L). [6]

The E–E model employs the volume-averaged mass and momentum conservation equations to describe the time-dependent motion of both phases. The bubbles in a computational cell are represented by a volume fraction. On the other hand, the E–L model adopts a continuum description for the liquid phase and additionally tracks each bubble using Newtonian equations of motion. This allows for a direct consideration of additional effects related to bubble–bubble and bubble–liquid interaction. Unlike the E–E model, the E–L model does not require additional models to predict the bubble size distribution since this information is already part of the solution. [6]

However, it is still pointed out that numerical diffusion can be a problem in the calculation of continuous phases even when using the E-L method. [7] Therefore, in order to resolve this problem, we adopted an approach that can eliminate numerical diffusion in the analysis between two phases by introducing Lagrangian analysis in the analysis of the continuous phase.

The DBM method was first introduced by Delnoij et al. [5] and is basically applied to a dispersed regime targeting relatively small bubbles that are constant in size and do not coalesce or break up. Each bubble is tracked by the following equations of motion.

$$\rho_g V_g \frac{d\vec{u}_g}{dt} = \vec{F}_{g,ext} \tag{2}$$

where, $\rho_g, V_g, \vec{u}_g$ and $\vec{F}_{g,ext}$ are the density of the gas phase, the volume and velocity of a bubble, and the total force acting on a bubble, respectively.

$$\vec{F}_{g,ext} = \vec{F}_G + \vec{F}_D + \vec{F}_L + \vec{F}_P + \vec{F}_V + \vec{F}_T + \vec{F}_W \tag{3}$$

Each of these forces is assumed to be independent and uncoupled from each other. Detailed expressions of these forces can be found in Table 3.

Based on the terminal rising velocity of a bubble, many researchers, including Ishii and Zuber and Tomiyama, expressed the drag coefficient of the bubble

Table 2. The forces and correlations acting on a particle.

$$\vec{F}_G = \rho_s V_s \vec{g}$$

$$\vec{F}_D = \frac{1}{8}\rho_l \pi d^2 \left|\vec{v}_l - \vec{v}_s\right|\left(\vec{v}_l - \vec{v}_s\right)\left\{\hat{f}^d\left(\varepsilon_l, R_{Es}\right)\frac{24}{R_{Es}}\right\}$$

$$C_D = \frac{24}{R_{Es}}\left\{1 + R_{Es}^{0.0964+0.5565\Psi} e^{2.3288-6.4581\Psi+2.4486\Psi^2}\right\}$$

$$+\frac{R_{Es}e^{4.905-13.8944\Psi+18.4222\Psi^2-10.2599\Psi^3}}{R_{Es}+e^{1.4681+12.2584\Psi-20.7322\Psi^2+15.8855\Psi^3}} \quad (\Psi: \text{sphericity})$$

$$\hat{f}^d\left(\varepsilon_l, R_{Es}\right) = \frac{C_D}{24}R_{Es}\varepsilon_l^{-\chi}$$

$$\chi = 3.7 - 0.65e^{-0.5\left(1.5-\log_{10}R_{Es}\right)^2}$$

$$\vec{F}_L \approx \frac{1}{8}\left(C_{L\omega} + C_{L\Omega}\right)\rho_l \pi d_s^2 \left|\vec{u}_s - \vec{u}_l\right|^2 \frac{\left(\nabla\times\vec{u}_l\right)\times\vec{u}_l}{\left|\left(\nabla\times\vec{u}_l\right)\times\vec{u}_l\right|}$$

$$C_{L\omega} = \begin{cases} \frac{18}{\pi^2}\left(\frac{S_r}{R_{Es}}\right)^{1/2} J(\varepsilon) - \frac{11}{8}S_r e^{-0.50R_{Es}} & \left(R_{Es} \le 50\right) \\ -0.064e^{0.525S_r}\left[0.49 + 0.51\tanh\left\{5\log\left(\frac{R_{Es}S_r^{0.08}}{120}\right)\right\}\right] & \end{cases}$$

$$C_{L\Omega} = R_r\begin{bmatrix} 1 - 0.62\tanh\left(0.3R_{Es}^{1/2}\right) \\ -0.24\tanh\left(0.01R_{Es}\right)\coth\left(0.8R_r^{1/2}\right)\arctan\left\{0.47\left(R_r - 1\right)\right\} \end{bmatrix}$$

$$R_r = \frac{\Omega d_s}{\left|\vec{u}_l - \vec{u}_s\right|} \qquad S_r = \frac{\left|\vec{\omega}\right| d_s}{\left|\vec{u}_l - \vec{u}_s\right|} \qquad f_{\omega\Omega} = 2\frac{R_r}{S_r}$$

$$\vec{F}_P = -V_s \nabla p$$

$$\vec{F}_V = \varepsilon_s \rho_l C_V\left(\frac{D\vec{u}_l}{Dt} - \frac{D\vec{u}_s}{Dt}\right)$$

$$\vec{F}_T = -\frac{3}{4}\frac{C_D}{d_s}\left|\vec{u}_l - \vec{u}_s\right|\frac{\mu_l^e}{S_C}V_s\varepsilon_s\left(\frac{1}{\varepsilon_l} + \frac{1}{\varepsilon_s}\right)\nabla\varepsilon_s$$

Table 3. The forces and correlations acting on a bubble.

$$\vec{F}_G = \rho_g V_g \vec{g}$$

$$\vec{F}_D = \frac{1}{8}C_D \rho_l \pi d_g^2 \left|\vec{u}_l - \vec{u}_g\right|\left(\vec{u}_l - \vec{u}_g\right)$$

$$C_D = C_{D\infty}\left(e^{3.64\varepsilon_g} + \varepsilon_g^{0.864}\right)$$

contaminated system:

$$C_{D\infty,\mathrm{TC}} = \max\left\{\frac{24}{R_{Eg}}\left(1 + 0.15R_{Eg}^{0.687}\right), \frac{8}{3}\frac{E_{\ddot{O}}}{E_{\ddot{O}} + 4}\right\}$$

$$\vec{F}_L = \rho_l V_g C_L\left(\vec{u}_l - \vec{u}_g\right)\times\left(\nabla\times\vec{u}_l\right)$$

$$C_L = \begin{cases} \min\left\{0.288\tanh\left(0.121R_{Eg}\right), f\left(E_{\ddot{O}}^H\right)\right\} & E_{\ddot{O}}^H < 4 \\ f\left(E_{\ddot{O}}^H\right) & 4 \le E_{\ddot{O}}^H < 10 \\ -0.27 & 10 \le E_{\ddot{O}}^H \end{cases}$$

$$f\left(E_{\ddot{O}}^H\right) = 0.00105E_{\ddot{O}}^{H3} - 0.0159E_{\ddot{O}}^{H2} - 0.0204E_{\ddot{O}}^H + 0.474$$

$$E_{\ddot{O}}^H = E_{\ddot{O}}\left(1 + 0.163E_{\ddot{O}}^{0.757}\right)^{2/3}$$

$$\vec{F}_P = -V_g \nabla p$$

$$\vec{F}_V = \varepsilon_g \rho_l C_V\left(\frac{D\vec{u}_l}{Dt} - \frac{D\vec{u}_g}{Dt}\right)$$

$$\vec{F}_T = -\frac{3}{4}\frac{C_D}{d_g}\left|\vec{u}_l - \vec{u}_g\right|\frac{\mu_l^e}{S_{\mathrm{Cg}}}V_g\varepsilon_g\left(\frac{1}{\varepsilon_l} + \frac{1}{\varepsilon_g}\right)\nabla\varepsilon_g$$

$$\vec{F}_W = \left(\frac{2\rho_l V_g}{d_g}\right)\left(\frac{d_g}{2y}\right)^2 C_W\left|\left(\vec{u}_l - \vec{u}_g\right)\vec{k}\right|^2\vec{n}_W$$

$$C_W = \begin{cases} e^{-0.933E_{\ddot{O}}+1.79} & 1 \le E_{\ddot{O}} < 5 \\ 0.007E_{\ddot{O}} + 0.04 & 5 \le E_{\ddot{O}} < 33 \end{cases}$$

as a function of the Reynold number (R_{Eg}) and the $E_{\ddot{O}}$ number. In this study, Tomiyama's model (for a contaminated system) was adopted for drag coefficient calculation, and Rusche's model which uses the volume faction around the bubble as a function to consider the effect of interaction between neighboring bubbles was used.

To consider the lift force perpendicular to the direction of relative motion between the bubble and the fluid, the lift coefficient correlation proposed by Tomiyama was used. The wall effect force, which is the force acting on the bubble moving near the wall, and the turbulent dispersion force proposed by Burns were also considered.

3.4 Interphase coupling

The unresolved approach uses a length scale for the continuous phase that is similar to or larger than that of the dispersed phase and uses empirical correlations to determine the force transmitted between the two phases.

This approach is suitable for analyzing the interaction behavior of many particles/bubbles over a relatively large domain. Basically, the unresolved approach uses the Navier-Stokes equations with local averaging technique for analyzing the continuous phase. [4][8]

In this study, for accurate volume fraction calculation using the gridless particle-based method, the method of directly calculating the volume defined by the overlap between the virtual sphere defined by the coupling radius and an arbitrary sphere was used. [10]

4. Numerical analysis

The code was written in CUDA v12.2 environment to run on GPUs such as Nvidia RTX3090 or RTX4090. Four Cell-Linked Lists (CLL) were used to enable all particles defining each phase to search for their neighboring particles quickly and efficiently. Parallelization using multiple GPUs was not implemented; instead, a single GPU was used for each calculation.

In advance of the simulations, the following three-step process was performed.

In the first step, we modeled a tank with the same conditions as the experiment and generated 69,191 MPS particles to analyze the liquid. After generating the MPS particles, we performed the analysis for about 10 seconds until the motion due to the interaction was sufficiently stabilized.

In the second step, 512 seed points were defined at the same locations as the experiment to generate bubbles according to each condition inside the liquid stabilized by the previous step, and bubbles were generated at appropriate time intervals to match the amount of bubbles generated per unit time. According to Kim et al. [2], the image measured by a high-speed camera at the center of the bubble column was analyzed and the bubbles were non-spherical shapes (flattened ellipsoid) and when converted to the equivalent-volume sphere diameter, it was measured as approximately 20.4 mm, with a standard deviation of 2.9 mm. Therefore, for simulation, bubbles with an average size of 19 mm and a maximum deviation of 1.0 mm were generated in the center, with an average size of 13.2 mm and a maximum deviation of 0.69 mm for the periphery, and with an average size of 12 mm and a maximum deviation of 0.63 mm for the outermost part by a random variable that followed a uniform distribution. To control the amount of bubbles generated per unit time, the amount of bubbles generated from each seed was recorded for a sufficiently long time, and the generation of bubbles was controlled so that a specified amount was generated for each seed. The calculation was performed for up to 120 sec. so that the bubble column and the flow field could be fully developed.

In the third step, in order to model the release of particles through the funnel, a hollow cylinder with a diameter (50 mm) and a length sufficiently larger than the outlet diameter (14.5 mm) of the funnel was modeled, and a fixed number of solid particles was generated inside and then dropped by gravity to form a stockpile. When the actual analysis began, this stockpile was translated at a specified speed, and when it reached a condition below a certain height, each particle was allowed to undergo particle-particle and particle-wall collision analysis. In this way, after being released from the stockpile state, the particles were allowed to fall a short distance, collide with the wall of the funnel, and then fall naturally through the outlet, so that the particles could behave as similarly as possible to the experiment. Just like the air flow rate for bubble generation, the mass of particles released per unit time is also expected to influence the result of the settlement of particles directly. The reason for colliding a pre-generated stockpile into the funnel instead of directly filling and releasing particles inside the funnel is to satisfy the condition of following the release rate in Table 1 exactly.

5. Results

As in the DAVINCI SG experiments, 25 simulations were performed with 5 air flow rates and 5 types of particles, and the mass of the particles collected in the particle catcher was investigated in the radial direction. Fig. 3 shows the comparison of particle sizes at the same time when the air flow rate used to generate the bubbles was 50 lpm. The larger the particle size, the less sensitive it is to the bubble effect and more concentrated in the center, while the smaller the particle size, the more sensitive it is. Fig. 4 shows the results of comparing the behavior of particles and bubbles at the same time according to 5 air flow rates for D_V1.95 particles. The particles are more strongly dispersed on the bottom surface as the bubble-induced effect increases.

Fig. 5 shows the radial mass distribution obtained from 20 simulations according to particle type and air flow rate. (No comparison was made since experimental results for D_V1.95 were not given.) Except for the case of 90 lpm air flow rate and small particles (D_V0.92 and D_V3.43), the results generally show similar trends to those obtained in the experiment. When the air flow rate is 0 lpm, the particle dispersion in the numerical result is somewhat lower than in the experiment. This suggests that the effect of particle-induced turbulence applied in the simulation is somewhat low, and it seems necessary to modify the model through more diverse experiments.

Fig. 6 to 8 show the comparison between MT2 experiments, in which five types of particles were mixed in a certain ratio, and the simulation results. As shown in Fig. 7, the mass distributions of settled particles in the radial direction by simulation seem similar to the experimental results. Fig. 8 compares the composition ratio of the particles captured in the central 40x40mm area. Except for the case Q_B90, the simulation results are similar to the experiment.

6. Conclusions

In an unresolved method, we coupled MPS, DEM, and DBM using a fully Lagrangian approach to simulate the collision of the bubble column generated by air injection with the particle column formed by falling debris particles. The quantitative measurement results obtained in the DAVINCI experiment were directly compared with the simulation results. Although there is a lot of uncertainty in experiments and simulations due to the complex behavior of many bubbles and particles by numerous collisions and the resulting complex fluid flow, the simulation results agreed well with few exceptions and showed similar trends to the experiments.

Even though the experiment was conducted under strictly controlled conditions and environments, the results of this experiment are expected to have some uncertainty.

According to Kim et al. [2], the bubbles measured at the center of the bubble column were non-spherical shapes (flattened ellipsoid), and under these conditions, a single bubble's rising trajectory instability occurs. It is known that the causes are the effects of the continuous shape instability of the bubble, the effects of the wake caused by the rising of the bubble, and the effects of contaminants contained in the liquid on the bubble surface. This is distinguished separately from the lift caused by the velocity gradient. Due to this rising trajectory instability, the bubble's path becomes uncertain, which affects the flow field and ultimately causes uncertainty in the falling trajectory of the falling particle.

Freely falling particles maintain their own angular velocities while passing through the funnel through particle-particle and particle-wall friction and collision processes. The angular velocity of particles at the moment of initial entry becomes the initial conditions that induce the lift of the particles and thus affect the initial behavior of the particles after entry, which is expected to affect the falling trajectories of the particles.

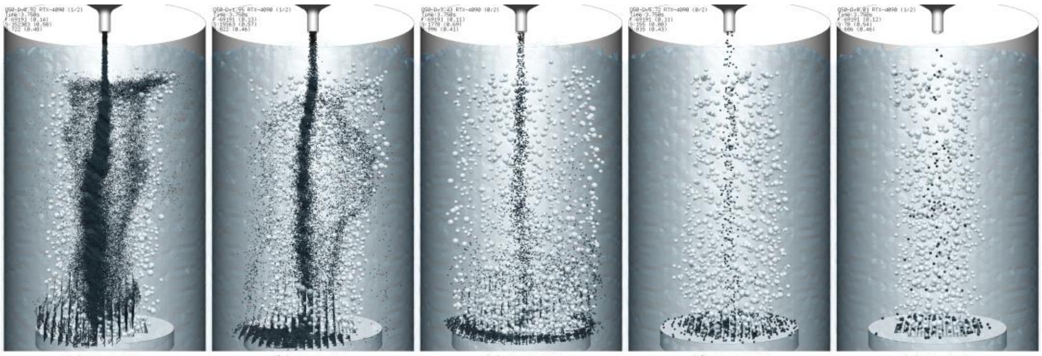

(a) D_V0.92 (b) D_V1.95 (c) D_V3.43 (d) D_V5.72 (e) D_V8.01

Fig. 3. Simulation snapshots of SG experiment: air flow rate 50 lpm. (T=3.75sec.)

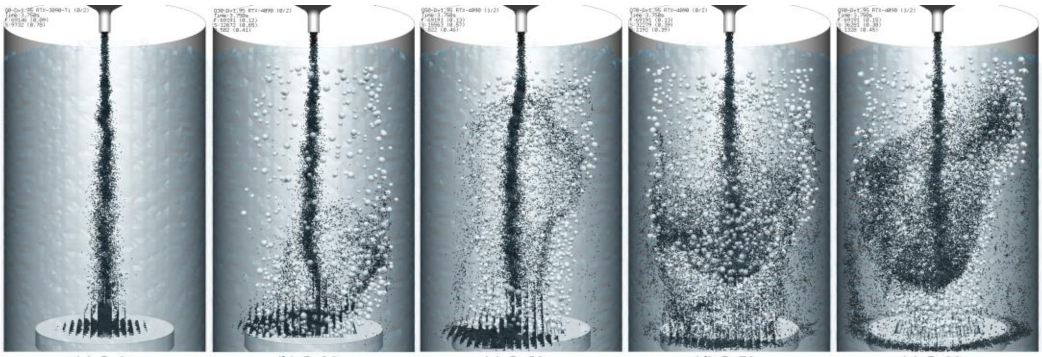

(a) Q_B0 (b) Q_B30 (c) Q_B50 (d) Q_B70 (e) Q_B90

Fig. 4. Simulation snapshots of SG experiment: D_V1.95. (T=3.75sec.)

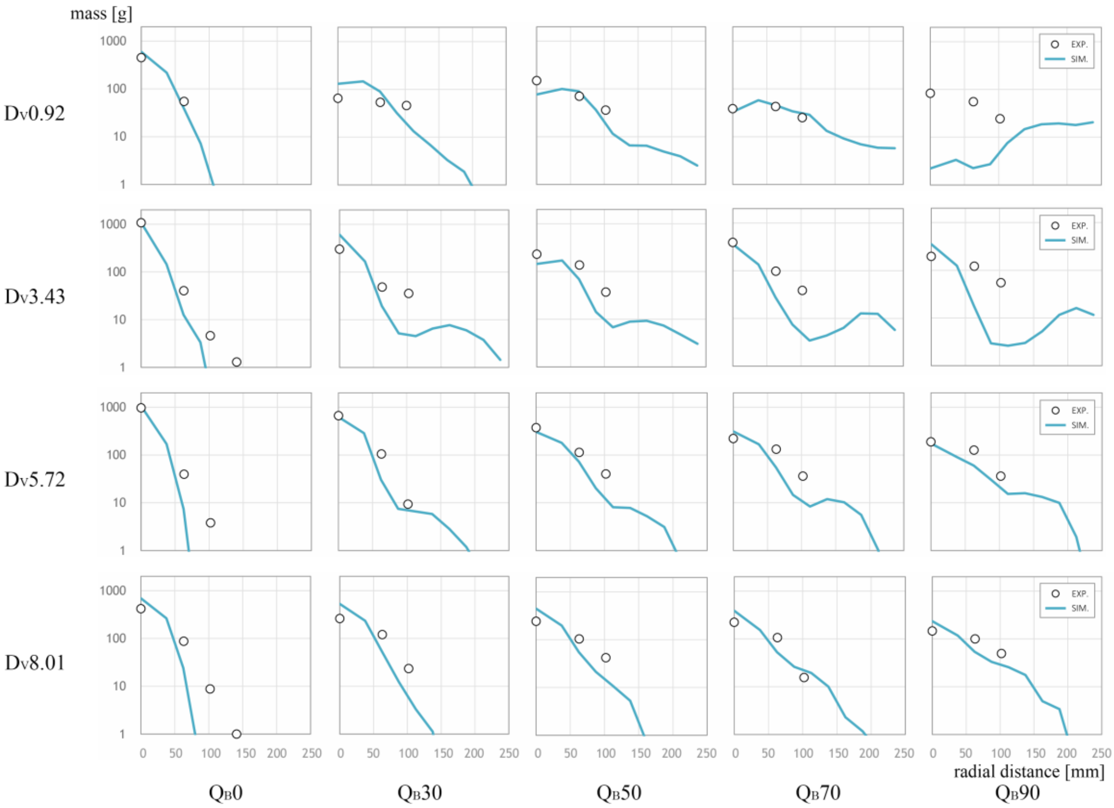

Fig. 5. Comparisons of mass of settled particles in radial distance in SG experiments and simulations.
(No comparison was made since experimental results for D_V1.95 were not given.)

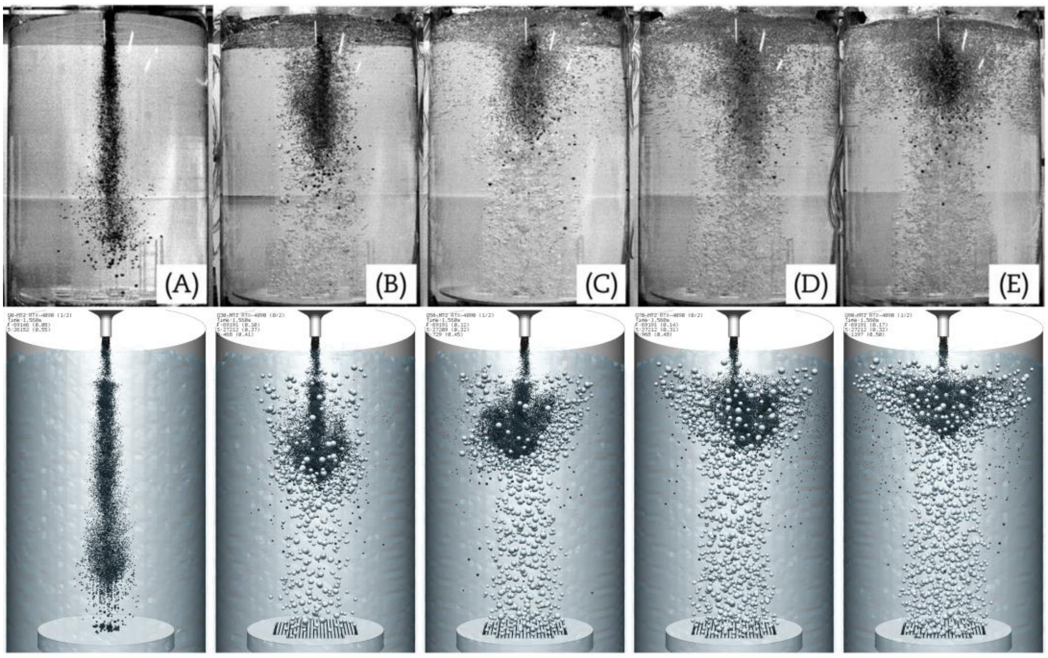

(a) MT2-Q_B0 (b) MT2-Q_B30 (c) MT2-Q_B50 (d) MT2-Q_B70 (e) MT2-Q_B90

Fig. 6. Snapshots of MT2 experiments (up) and simulations (down) for 5 air flow rate conditions.

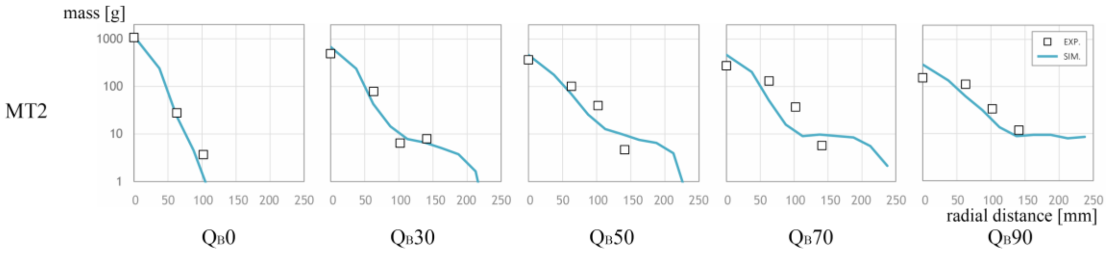

Fig. 7. Comparisons of mass of settled particles in radial distance in MT2 experiments and simulations.

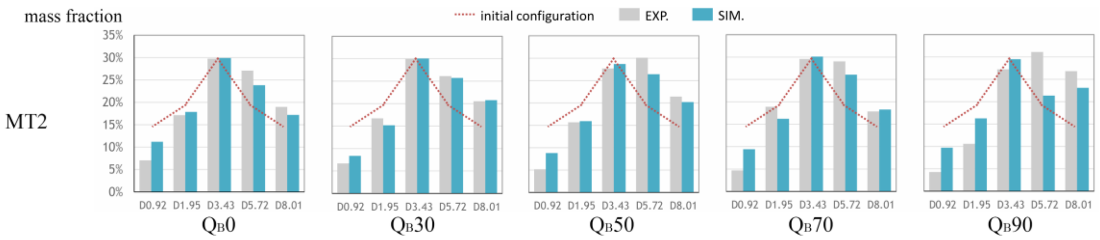

Fig. 8. Particle size distributions at the center region (40x40 mm) in MT2 experiments and simulations.

The following limitations are pointed out in the numerical analysis.

First, the coalescence and breakup of bubbles were not considered in this study. When a rising bubble and a falling particle collide, it is expected that a large bubble will be separated into small bubbles, and it is expected that two rising bubbles will be regenerated into one bubble if certain conditions are met. However, research on this phenomenon is not yet sufficient, and although some researchers have attempted numerical analysis approaches, it seems that a clear model has not yet been established.

Second, the drag and lift forces calculated in dispersed phases such as bubbles and particles are steady forces, and unsteady forces are not considered. Research on this unsteady force is also insufficient, and it is pointed out that it has not been established yet, or numerical implementation requires a huge amount of memory and calculation. [8]

Third, the correlation used to obtain the lift force of particles is for spherical particles, and sphericity for expressing non-spherical particles is not considered.

Fourth, the turbulent Schmidt number used in calculating the turbulent dispersion of the dispersed phase is not a property of the liquid and is dependent on the state, so it is difficult to determine an appropriate constant value. This value can only be estimated as an appropriate value through experiments.

The difference between the experimental and numerical results should be understood by considering the uncertainties of the phenomenon and the limitations of the numerical analysis mentioned above.

REFERENCES

[1] E. Kim, W. Jung, J. Park, H. Park, and K. Moriyama, Experiments on Sedimentation of Particles in a Water Pool with Gas Inflow, Nuclear Eng. and Tech., Vol. 48, pp. 457-469, 2016.
[2] E. Kim, Debris Bed Formation during Ex-Vessel Severe Accidents in Light Water Reactors, Doctoral Thesis, Pohang University of Science and Technology, 2016.
[3] Y. Jo, S. Park, and E. Kim, Numerical Simulation of 3-Phase Debris Bed Hydrodynamic Leveling Behavior Using Multi-Phase SPH-DEM Coupling, Trans. of the Korean Nuclear Soc. Virtual Spring Meeting, 2022.
[4] Y. Jo, S. Park, H. Yoo, and E. Kim, GPU-based SPH-DEM Method to Examine the Three-Phase Hydrodynamic Interactions between Multiphase Flow and Solid Particles, Int. J. of Multiphase Flow, Vol. 153, 2022.
[5] E. Delnoij, J.A.M. Kuipers, and W. Van Swaaij, A three-dimensional CFD model for gas–liquid bubble columns. Chem. Eng. Sci., Vol. 54, pp. 2217–2226, 1999.
[6] D. Darmana, N.G. Deen, and J.A.M. Kuipers, Detailed modeling of hydrodynamics, mass transfer and chemical reactions in a bubble column using a discrete bubble model, Chem. Eng. Sci., Vol. 60, pp. 3383–3404, 2005.
[7] S. Koshizuka, K. Shibata, M. Kondo, and T. Matsunaga, Moving Particle Semi-Implicit Method, Academic Press, 2018. with a generic wall boundary condition, Computers and Fluids, Vol. 178, pp. 88-112, 2019.
[8] H. Norouzi, R. Zarghami, R. Sotudeh-Gharebagh, and N. Mostoufi, Coupled CFD-DEM Modeling: Formulation, Implementation and Application to Multiphase Flows, Wiley, 2016.
[9] A. Haider, and O. Levenspiel, Drag coefficient and terminal velocity of spherical and nonspherical particles, Powder Tech., Vol. 58, pp. 63-70, 1989.
[10] Y. Son, C. Ahn, S. Lee, Using a Lagrangian-Lagrangian Approach for Studying Flow Behavior Inside a Bubble Column, Nuclear Eng. and Tech., Vol. 55, pp. 4395-4407, 2023.